EDGE ARTICLE

Check for updates

All publication charges for this article have been paid for by the Royal Society of Chemistry

Controllable synthesis of a chemically stable molecular sieving nanofilm for highly efficient organic solvent nanofiltration†

Yi Li, [ID] [a] Sha Li, [ID] *[b] Junyong Zhu, [ID] [c] Alexander Volodine[d] and Bart Van der Bruggen*[ae]

Membranes with versatile separation capacity and strong chemical resistance are necessary for organic solvent nanofiltration (OSN). Here, a molecular sieving nanofilm with Janus pore structures was synthesized by introducing alkyl ($-CH_2-$) moieties into the hydrophilic cross-linked polyamide network. *In situ* interfacial polymerization between *m*-xylylenediamine (*m*-XDA) and trimesoyl chloride (TMC) monomers was manipulated on a solvent-resistant nanofibrous hydrogel substrate. By varying monomer concentrations, thin film composite (TFC) OSN membranes were achieved with tuneable nanofilm thickness and hydrophobicity. Janus pathways in the *m*-XDA/TMC molecular sieving nanofilm contribute to a high solvent permeability for both polar and non-polar solvents; for example, for acetone the permeability is 8.2–54.5 L m^{-2} h^{-1} bar^{-1}, for *n*-hexane 0.6–2.6 L m^{-2} h^{-1} bar^{-1}, and for toluene 4.2 L m^{-2} h^{-1} bar^{-1}. The composite membrane revealed a molecular weight cut-off of 242–327 g mol^{-1} in both acetone and methanol. Moreover, the membrane exhibited chemical and structural stability after immersing it in both strongly acidic or strongly basic environments for 15 days. This outstanding chemical stability, combined with the excellent permeability and selectivity, makes the *m*-XDA/TMC composite membrane a promising candidate for versatile OSN applications in polar and non-polar solvents as well as under extreme conditions.

1. Introduction

Organic solvent nanofiltration (OSN) has attracted increasing interest in a wide range of applications in chemical processes, such as solvent recycling, concentration and solute extraction.[1–3] The OSN membrane can effectively fractionate solutes with a molecular weight (MW) between 200 and 1000 Da from organic liquids.[2–4] This requires the membrane to be tolerant to harsh organic media in a complex background (strong acid/base, high temperature, aggressive solvent, and polar/non-polar solvents).[4–6] Thus, membranes with a versatile separation capability and a strong chemical resistance are highly desirable for organic solvent separations.

Thin film composite (TFC) membranes are typical organic solvent nanofiltration membranes, consisting of a selective layer, a polymeric substrate and a non-woven fabric support.[7] Due to their stability in organic solvents and superior separation efficiencies as well as the designable pore architecture of the skin selective layer, TFC membranes are preferred.[8] However, conventional polyamide membranes developed from monomers of *m*-phenylenediamine (MPD) and trimesoyl chloride (TMC) through interfacial polymerization (IP) are particularly unsuitable for non-polar solvents, such as *n*-hexane, due to their highly cross-linked chemical structure and intrinsic hydrophilicity prohibiting solvent transport.[9,10] In applications, organic solvent systems are sophisticated as they contain both polar and non-polar solvents.[4,10] Currently, most OSN membranes are only suitable for either polar or non-polar organic solvents.[8,10–13] Incorporation of fluorine and silicon in the polyamide top layer can effectively endow the membrane with hydrophobic properties.[9] However, the grafting barrier layer inevitably decreases the solvent permeability due to the resulting higher resistance. Furthermore, the dense structure of the top selective layer still poses a challenge. Recently, molecule-level design strategies have been shown to be promising in manipulating the pore structure and its physicochemical properties towards highly permeable OSN membranes.[5,10–12,14–16] For example, Chung *et al.* constructed

[a]Department of Chemical Engineering, KU Leuven, Celestijnenlaan 200F, B-3001, Leuven, Belgium. E-mail: bart.vanderbruggen@kuleuven.be

[b]Department of Bioengineering, Zhuhai Campus of Zunyi Medical University, Zhuhai, Guangdong 519041, P. R. China. E-mail: lisha_jnu@163.com

[c]School of Chemical Engineering and Energy, Zhengzhou University, Zhengzhou 450001, P. R. China

[d]Department of Physics and Astronomy, KU Leuven, Celestijnenlaan 200 D, 3001 Leuven, Belgium

[e]Faculty of Engineering and the Built Environment, Tshwane University of Technology, Private Bag X680, Pretoria 0001, South Africa

† Electronic supplementary information (ESI) available. See DOI: 10.1039/d0sc00056f

Janus pathways with both hydrophobic and hydrophilic channels using cyclodextrins (CDs) as building blocks.[10] The hydrophobic inner cavities of CDs facilitate transport of non-polar solvent molecules and the hydrophilic outer space provides superhighways for polar solvent molecules. However, the large pore size of the CDs could only enable membrane rejection of large solute molecules. Liang *et al.* prepared conjugated microporous polymer (CMP) membranes *via* a surface-initiated polymerization strategy through C–C coupling reactions.[14] The rigid backbones of the CMP enable ultra-fast organic solvent nanofiltration. Nevertheless, the complex molecular manipulation poses challenges in industrial application. A facile method to construct a well-defined pore structure may open up new opportunities to design advanced OSN membranes for filtration of both polar and non-polar solvents. In addition, it is still a formidable challenge to achieve a membrane possessing high chemical and structural stability under harsh conditions. Recently, Liu *et al.* prepared a novel nanofiltration membrane by blending *m*-xylylenediamine (*m*-XDA) and polyethyleneimine as the aqueous co-monomer.[17] The addition of *m*-XDA endows the NF membrane with good chlorine-tolerant properties. The methylene of the *m*-XDA reduces the activity of amide bonds and improves the chemical resistance of the thin film.

Here we propose a new synthetic approach to designing molecular sieving nanofilms with Janus pore structures. An aromatic diamine with an "elongated arm" of the methylene moiety was used as the aqueous monomer for the interfacial polymerization. The methylene moiety introduced in the polyamide network endows the nanofilms with Janus pores containing both hydrophilic parts and hydrophobic parts. The surface morphology, thickness and hydrophilicity of the nanofilms were effectively controlled by varying the monomer concentrations. The solvent-resistant aramid nanofibrous hydrogel was used as a "green" support without further cross-linking. Nanofiltration of polar and non-polar organic solvents with the composite membranes was investigated. The excellent chemical stability of the composite membranes was also evaluated under both aggressive acidic and strongly basic conditions. This work demonstrates that interfacial synthesis using monomers of extended alkanes provides polymeric nanofilms with tunable structural diversity and chemical stability.

2. Experimental

2.1 Chemicals and materials

Kevlar in the form of fibers was obtained from Zhangjiagang Free Trade Zone Fengduo International Trade Co., Ltd., China. A non-woven support polypropylene/polyethylene (PP/PE) fabric Novatex 2471 was obtained from Freudenberg (Germany). Potassium hydroxide (KOH, 85%, Acros Organics NV) and dimethyl sulfoxide (DMSO, Acros Organics NV) were used to dissociate the Kevlar fiber. *m*-Xylylenediamine (*m*-XDA, 99%), trimesoyl chloride (TMC, 98%), triethylamine (TEA, 99%), methanol (99.9%), isopropanol (IPA, 99.5%), tetrahydrofuran (THF, 99.5%), acetone (99.9%), acetonitrile (99.9%), *N,N*-dimethylformamide (DMF, 99.8%) and 1-methyl-2-pyrrolidinone

(NMP, 99%) were purchased from Sigma-Aldrich BVBA. Ethanol and toluene were purchased from VWR International BVBA. Hydrochloric acid (HCl, ≥37%, aqueous solution, density: 1.190 g cm^{-3}) and sodium hydroxide (NaOH, 50% aqueous solution, density: 1.515 g cm^{-3}) were used to examine the membrane chemical stability. Dyes with different molecular weights and dimensional sizes were obtained from Sigma-Aldrich. All chemicals were used as received without further purification.

2.2 ANF hydrogel substrate preparation

The casting solution was prepared as reported previously.[2,17] The ANF hydrogel membrane was produced *via* non-solvent phase inversion in water. The casting solutions were allowed to settle to remove air bubbles and undissolved precipitates before casting the membrane. The non-woven polypropylene/polyethylene (PP/PE) or polyolefin (PO) fabric was placed on a clean glass plate. The casting solutions were cast onto the PP/PE support using a casting knife set to a thickness of 250 μm at a temperature of 20–25 °C. The hydrogel membranes precipitated from the water after phase inversion and were stored overnight in deionized (DI) water.

2.3 Freestanding nanofilm and *m*-XDA/TMC composite membrane preparation

A freestanding *m*-XDA/TMC molecular sieving nanofilm was prepared on the support-free water/hexane interface *via* interfacial polymerization. The *m*-XDA/TMC molecular sieving nanofilm was *in situ* fabricated on the ANF hydrogel substrate by interfacial polymerization as follows. Firstly, the hydrogel support membrane was purged with nitrogen gas to remove the water on the membrane surface. Subsequently, the aqueous diamine solution containing *m*-XDA and 0.5 wt% TEA was poured onto the hydrogel membrane surface and kept for 6 min. After draining the aqueous solution, the residual droplets were absorbed gently using a tissue paper and the membrane was dried for 1–3 min. Then, the organic hexane containing TMC was poured on the membrane surface to form a selective polyamide layer. The organic solution was drained after 1 min of reaction and the membrane surface was rinsed with pure hexane. Finally, the resulting membrane was cured in an oven at 90 °C for 1 min to enhance the crosslinking reaction and immediately placed in DI water for storage. The as-prepared membrane was denoted as *m*-XDA/TMC-*x/y*, where *x* represents the concentration of *m*-XDA in the aqueous solution and *y* indicates the concentration of TMC in the organic phase.

2.4 Characterization

The morphology of the membrane surface and of the cross-section was observed using a XL30 FEG field-emission scanning electron microscope (FE-SEM, the Netherlands). Each sample was sputter-coated with a 1.5–2 nm Au layer before testing. Atomic force microscopy (AFM) was performed under ambient conditions using a Dimension 3100D AFM (Bruker) to obtain the membrane surface morphology, roughness and membrane thickness. The thickness of the freestanding

nanofilms was measured by depositing the nanofilm on a silica substrate. AFM images were obtained in tapping mode using SSS-NCHR probes from NanoAndMore GmbH. The cantilever was made of Si with a spring constant of 40–50 N m^{-1} and a nominal tip apex radius of <5 nm. The AFM images were flattened with order 1 after scanning. After flattening, the roughness parameter was calculated using the ISO 25178-2 standard. The elemental compositions of the m-XDA/TMC composite membrane were determined using X-ray photo-electron spectroscopy (XPS, AXIS Ultra DLD, Kratos Analytical, Japan). The acquisition time was 321 s, the anode was mono (aluminium (mono); 45 W), the step was 50.0 meW and the dwell time was 200 ms. The charge neutralizer was set at: current 1.8 A, balance 3.3 V and bias 1.0 V. X-ray diffraction (XRD) analysis was utilized to examine the crystalline structure of the prepared composite membranes using a Philips PW1830 diffractometer with a Bragg/Brentano θ–2θ setup and CuKα radiation at 45 kV to 30 mA on a 173 mm goniometer circle. The chemical structures of the composite membrane surfaces were analyzed by attenuated total reflectance Fourier transform infrared spectroscopy (ATR-FTIR, NEXUS670). The contact angles were measured with a 3.0 μL DI water drop using the sessile drop method on a video contact angle system (OCA20, Dataphysics, German). The average value of six measurements at random positions for each sample was reported. The surface charge of the membranes was measured using the zeta poten-tial (SurPASS 3, Anton Paar, Australia) with a 1 mM KCl elec-trolyte solution; the pH was adjusted with 0.05 mol L^{-1} HCl and NaOH and the gap height was fixed at 100 μm. The thin film made from m-xylylenediamine (m-XDA) and trimesoyl chloride (TMC) from an interfacial reaction is presented in Fig. S1.† The degree of network cross-linking (DNC) is the fraction of fully cross-linked segments in the polymer thin film as defined in eqn (1) and (2):[12]

$$\text{DNC} = \frac{X}{X + Y} \times 100\% \tag{1}$$

$$X + Y = 1 \tag{2}$$

where X and Y are the crosslinked segments and the linear segments in the polyamide network. According to the chemical formula of fully cross-linked ($C_{21}O_3H_{18}N_3$) and fully linear ($C_{17}O_4H_{14}N_2$) polyamide, the theoretical O/N ratio can be pre-sented by:[12]

$$\frac{O}{N} = \frac{3X + 4Y}{3X + 2Y} \tag{3}$$

The O/N element ratios were determined from the respective peak areas from XPS narrow scan elemental peaks. Based on eqn (3), the DNC of the m-XDA/TMC thin film was calculated.

2.5 Evaluation of OSN performance

The separation performance of prepared membranes was eval-uated in a stainless-steel dead-end membrane module (HP4750) with an effective testing membrane area of 14.6 cm^2. The

separation equipment was operated with a constant stirring of 600 rpm to minimize concentration polarization at 20–25 °C. The organic solvent nanofiltration performance of the membrane was evaluated in various organic solvents using different dyes with a concentration of 20 mg L^{-1} at 4 bar. In all the OSN experiments, the membranes were filtered with pure DMF for 10 min to activate the membrane, followed by filtration of pure acetone for 10 min before testing. The solvent perme-ability (P, L m^{-2} h^{-1} bar^{-1}) was calculated from the following equation:

$$P = \frac{V}{A \times t \times \Delta P} \tag{4}$$

where V is the volume of the collected permeate (L), A is the effective area of the testing membrane (m^2), t is the interval time (h) and ΔP is the applied transmembrane pressure (bar).

The solute (dye or salt) rejections (R, %) were calculated using the following equation:

$$R = \left(1 - \frac{C_p}{C_f}\right) \times 100\% \tag{5}$$

where C_p and C_f are the solute concentrations in the permeate and feed solutions, respectively. The dye concentrations were determined using a PerkinElmer lambda 12 UV-vis spectrophotometer.

2.6 Chemical stability test

The long-term filtration stability test of the membrane in aggressive acetone was evaluated using methyl orange (327 g mol^{-1}) as the solute with a concentration of 100 mg L^{-1} at 4 bar and 600 rpm in dead-end filtration in batch mode for seven cycles. For each cycle, the membrane was tested for 8 hours and allowed to stand undisturbed for 16 hours. The feed solution was 200 mL and the permeate was recycled when collecting 100 mL. As the feed organic stream in practical applications generally involves highly harsh conditions,[1,5,18] the chemical stability of the m-XDA/TMC composite membranes under harsh acidic and basic conditions was also investigated. The membranes were cut into disks (5 cm in diameter) and immersed in 30 mL of 0.1 M and 0.5 M HCl water/ethanol, 0.1 M and 0.5 M NaOH water/ethanol, and 0.1 M, 0.5 M, and 1 M HCl water/acetone, respectively for 15 days. The detailed composi-tions of the acid/organic and base/organic are listed in Table S1.† After this, the OSN performance of the treated membrane was evaluated using methanol and acetone as the feed solution and using dye molecules as the solute with a concentration of 20 mg L^{-1} in dead-end filtration at a pressure of 4 bar and 600 rpm. The membrane was rinsed with DI water for 5 min to remove the residual solution mixture and filtered with DMF for 10 min before testing.

3. Results and discussion

3.1 Fabrication of m-XDA/TMC membranes

Fig. 1a illustrates the interfacial polymerization (IP) process on the aramid nanofiber (ANF) hydrogel substrate. Due to the interconnected porous structure, the nanofibrous substrate
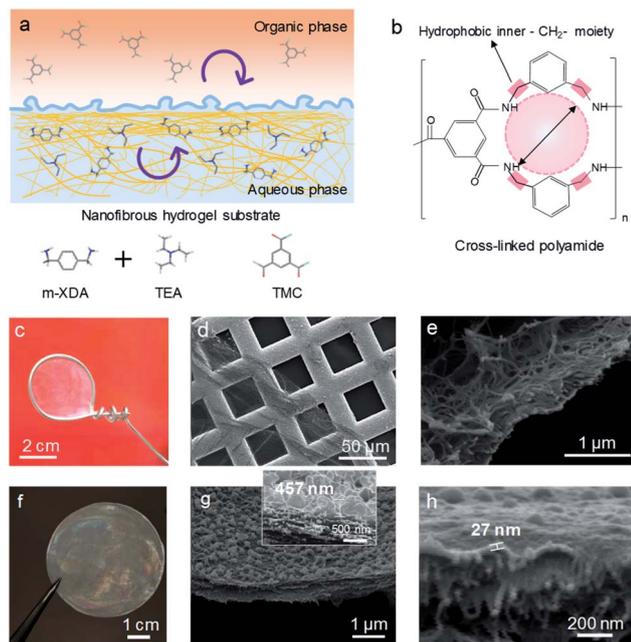
Fig. 1 Interfacial synthesis of hydrophobic polyamide nanofilms. (a) Visualization of the interfacial polymerization process on the ANF hydrogel substrate. (b) The planar structure of the synthesized polyamide. (c) Photograph of the nanofilm (∼100 nm) transferred to a steel wire lasso (m-XDA/TMC-2/0.1). (d) Large area SEM image of the nanofilm membrane on copper mesh (m-XDA/TMC-2/0.1). (e) Cross-sectional SEM image of the ANF substrate without the non-woven support. (f) A photograph of the m-XDA/TMC-3/0.15 composite membrane fabricated on an ANF hydrogel substrate (diameter: 5 cm) held by tweezers. (g and h) Cross-sectional SEM images of the m-XDA/TMC composite membranes. ((g) m-XDA/TMC-3/0.15; (h) m-XDA/TMC-0.5/0.025).

provides a homogeneous distribution of the aqueous solution compared to a conventional polymeric dense substrate.[2] In addition, the non-covalent interactions between water and the macromolecular chain of nanofibers controlled the diffusion of the aqueous solution.[2,19] A defect-free selective layer with an ultra-thin thickness is expected based on the ANF substrate. A molecular sieving nanofilm was prepared *via* IP between *m*-xylylenediamine (*m*-XDA) in aqueous solution and trimesoyl chloride (TMC) in the hexane phase. Triethylamine (TEA) was used as the additive in the aqueous solution to absorb the byproduct of HCl produced during IP, thereby enhancing the cross-linking degree of the selective layer.[20,21] *m*-XDA as an aromatic diamine was used as the aqueous monomer for the synthesis of the OSN membrane. It has a similar chemical structure to the commonly used *m*-phenylenediamine (MPD) (Fig. S2†). However, the methylene moiety (–CH₂–) situated between the benzene ring and the amide group is expected to endow the crosslinked polyamide (PA) nanofilm with hydrophobic properties (Fig. 1b). Besides, the elongated side chain could produce a larger membrane pore size compared to that of the nanofilms prepared from MPD/TMC. Fig. 1c displays the freestanding nanofilm held by a 4 cm diameter steel ring. Fig. 1d shows the SEM image of a crumpled and defect-free nanofilm prepared from the support-free water/hexane

interface, followed by transfer onto a copper mesh. Free-standing nanofilms prepared from different ratios of *m*-XDA/TMC could also be easily obtained (Fig. S3†). In view of industrial applications in pressure-driven organic solvent nano-filtration, a composite membrane containing a selective nanofilm and a porous substrate was fabricated. As shown in Fig. 1e, the intertwined aramid nanofibers were used as "building blocks" to create a robust 3D interconnected structure for the membrane substrate. The solvent-resistant fibrous substrate has a great advantage over conventional polymeric supports as it requires no cross-linking agent.[2] The molecular sieving nanofilm with the support of ANF hydrogel yields a colorful surface, indicating the successful interfacial polymerization (Fig. 1f).[2,19] The IP process on the hydrogel substrate was manipulated on a molecular level by varying the monomer concentration of *m*-XDA and TMC. As shown in Fig. 1g, the *m*-XDA/TMC-3/0.15 composite membrane exhibited a rough surface with a "leaf-like" structure and a high thickness of 457 nm (Fig. S4†). In addition, a smooth and ultra-thin selective layer with a thickness down to 27 nm was also obtained for the *m*-XDA/TMC-0.5/0.025 membrane (Fig. 1h).

In order to precisely control the membrane thickness, the monomer concentration was varied, manipulating the condensation rate and cross-linking degree. In this work, molecular sieving nanofilms were prepared by fixing the concentration ratio of *m*-XDA/TMC at 20 but varying the monomer concentrations (3/0.15, 2/0.1, 1.5/0.075, 1/0.05, and 0.5/0.025). The corresponding nanofilm thickness was between 27 and 457 nm. The nanofilm thickness was found to be inversely proportional to concentration levels (Fig. S4†). Moreover, the membrane surface morphology greatly varied depending on the monomer concentration (Fig. 2b–f and S5†). The ANF substrate was found to have a relatively rough surface (Fig. 2a). After interfacial polymerization, a dense and smooth thin film membrane covered the substrate (Fig. 2b). In addition, a growing number of crystalline particles were observed on the membrane surface, indicating an increased condensation reaction rate, as shown in Fig. 2b–e.[22] Notably, the membrane surface produced well distributed hollow bubbles at a monomer concentration of 3/0.15 (Fig. 2f). These bubbles are generated *in*
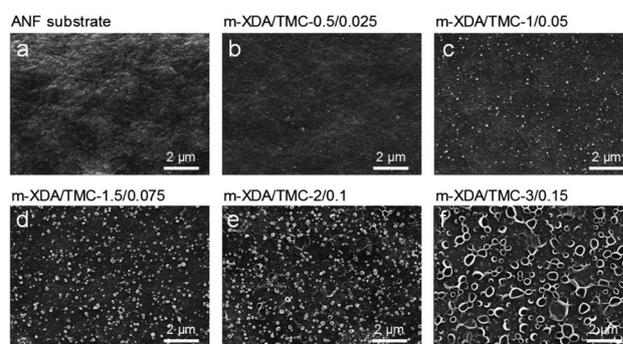

Fig. 2 SEM observations of membrane surface morphology. (a) ANF hydrogel substrate; (b) m-XDA/TMC-0.5/0.025; (c) m-XDA/TMC-1/0.05; (d) m-XDA/TMC-1.5/0.075; (e) m-XDA/TMC2/0.1; (f) m-XDA/TMC-3/0.15.

Table 1 Composition and surface physicochemical properties of the *m*-XDA/TMC composite membrane

Composite membrane	Overall thickness (nm)	RMS roughness (nm)	Atomic composition from XPS (%)				Degree of network cross-linking (%)	Contact angle (°)	Zeta potential (mV)
			C	N	O	O/N			
m-XDA/TMC-3/0.15	457 ± 72	42.7	80.1	8.5	11.4	1.34	56.4	55.3 ± 5.1	−38.15
m-XDA/TMC-2/0.1	105 ± 21	20.5	80.7	8.1	11.2	1.38	52.1	60.3 ± 3.0	−43.48
m-XDA/TMC-1.5/0.075	57 ± 16	16.0	81.1	7.9	11.0	1.40	50.0	66.2 ± 3.1	−35.83
m-XDA/TMC-1/0.05	40 ± 6	14.1	80.4	7.9	11.7	1.49	41.0	103.1 ± 5.1	−33.81
m-XDA/TMC-0.5/0.025	27 ± 9	16.5	81.8	7.5	10.7	1.43	46.9	98.3 ± 3.1	−24.77

situ by the heat released during interfacial polymerization due to the fast reaction rate at high monomer concentrations. The surface morphology and roughness of the composite membranes were also analyzed by atomic force microscopy (AFM), as shown in Fig. S6.† Table 1 shows that the *m*-XDA/TMC-3/0.15 membrane has the highest root-mean square (RMS) surface roughness of 42.7 nm, as compared to those scoring between 14 and 21 nm. These results are in accordance with the SEM images (Fig. 2).

3.2 Characterization

X-ray diffraction (XRD) was used to examine the chemical structure of the nanofilms. The results are shown in Fig. 3a. In comparison with the XRD pattern of the pristine silica substrate, the XRD pattern of the nanofilms shows two strong peaks at 2θ values of 7.8° and 15.3°. This indicates that the nanofilm has a crystalline structure.[22] The *m*-XDA/TMC-2/0.1 membrane and the *m*-XDA/TMC-1.5/0.075 membrane show a higher degree of crystallinity with values of 98.1% and 95.8%, respectively (Table S2†). However, the *m*-XDA/TMC-3/0.15 has the lowest crystallinity of 81.8%, which indicates a higher content of amorphous regions in the nanofilm. Karode *et al.* developed a comprehensive model for interfacial polymerization and found that film growth by nucleation is dominant as the organic phase concentration decreases.[23] Thus, the lower crystalline fraction of the *m*-XDA/TMC-3/0.15 membrane might be caused by the high organic phase concentration. In addition, a sufficiently high reactant concentration also leads to more rapid heat release from the exothermic polycondensation reaction, producing a more pronounced amorphous structure.[24] To demonstrate the successful interfacial polymerization between *m*-XDA and TMC, the membrane surface chemistry was examined by Fourier transform-infrared spectroscopy (FT-IR) (Fig. 3b). The *m*-XDA/TMC composite membranes show FT-IR spectra similar to that of the ANF hydrogel substrate, except for the two new peaks appearing at 2842 cm^{-1} and 2910 cm^{-1}, which originate from the C–H bending vibration of methylene (–CH$_2$–). This indicates that the –CH$_2$– was successfully introduced into the polyamide structure. The N–H stretching vibration at 3320 cm^{-1} is ascribed to the amine group.[3] The characteristic peaks at 1644 cm^{-1} (C=O stretching vibration, amide I band) and 1540 cm^{-1} (N–H in-plane bending and C–N bending vibration, amide II band) demonstrate the presence of functional –NHCO– bonds.[2,19] The elemental composition,

chemical bonding, and cross-linking degree of the molecular sieving nanofilm were analyzed by X-ray photoelectron spectroscopy (XPS). The XPS survey spectra of composite membranes presented in Fig. 3c confirm the presence of carbon (C 1s), nitrogen (N 1s) and oxygen (O 1s) elements at the membrane surfaces (∼10 nm depth). The cross-linking degree was calculated from the ratio of O/N (Table 1).[12] It was found that the *m*-XDA/TMC-3/0.15 membrane has the highest cross-linking degree (56.4%), followed by the *m*-XDA/TMC-2/0.1 membrane (52.1%). The synthetic components after deconvolution along with the background and fitted curves are shown in Fig. 3d–f. The C1s spectrum of the *m*-XDA/TMC-3/0.15
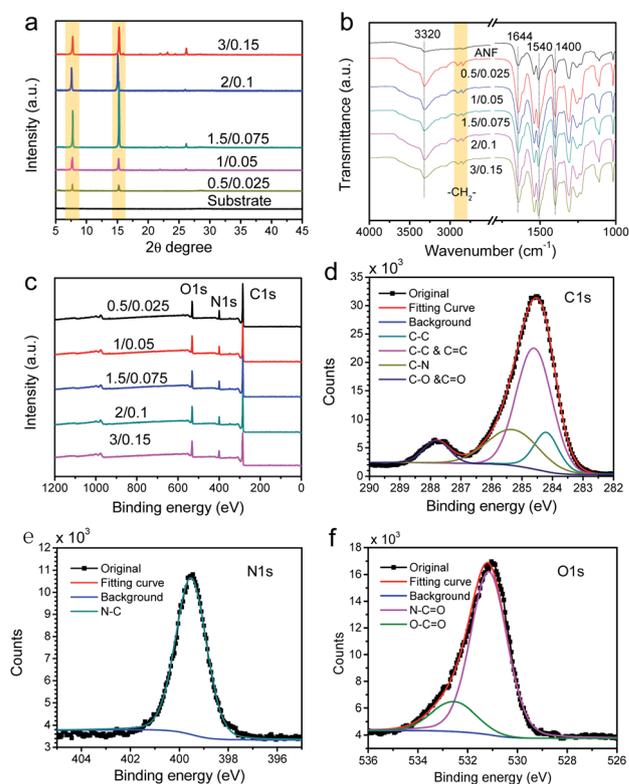

Fig. 3 (a) XRD patterns of the *m*-XDA/TMC nanofilms and silica wafer substrate (black). Nanofilms were prepared on the silica substrate. (b) FT-IR spectra of the composite *m*-XDA/TMC membranes and ANF substrate membrane. (c) XPS survey spectra of composite *m*-XDA/TMC membranes. (d–f) The C1s, N1s and O1s photoelectron spectra of the *m*-XDA/TMC-3/0.15 membrane prepared without TEA in the aqueous solution.

membrane without TEA addition (Fig. 3d) was deconvoluted into four peaks at 284.2 eV (C–C), 284.8 eV (C–C and C=C), 285.3 eV (C–N) and 287.8 eV (C–O and O–C=O).[2] The N 1s spectrum showed the amide bond at 399.5 eV (N–C=O) (Fig. 3e).[2] The O1s spectrum of the nanofilm was deconvoluted into two peaks at 531.2 eV and 532.6 eV, corresponding to the amide bond (N–C=O) and the carboxylic acid group (O–C=O), respectively (Fig. 3f).[25,26] The narrow scan results of the XPS spectra of composite membranes with the addition of TEA are shown in Fig. S7.† Plausible species for the polyamide composite membranes with the addition of TEA were determined from the deconvolution of C1s, O1s and N1s core level XPS spectra (Table S3†).

Because of the hydrolysis of residue acyl groups into carboxyl groups and the intrinsic hydrophilicity of polyamide, conventional TFC membranes prepared from MPD/TMC always have a hydrophilic surface, especially after the solvent activation of DMF.[9,19] This explains why PA membranes have no/extremely low permeance for non-polar solvents. As shown in Fig. S8,† compared with an m-XDA/TMC composite membrane, the polyamide thin film surface shows good wettability with a water contact angle (CA) of 33.2°. However, interestingly, introducing hydrophobic moieties into the cross-linked polyamide could effectively balance the hydrophilicity–hydrophobicity. It was found that reducing the m-XDA/TMC concentration could shift the composite membrane surface from hydrophilic to hydrophobic. As shown in Fig. 4a, the ANF substrate has a CA of 67.2°. Because of the higher content of the carboxyl groups (>2%) and amide groups (related to the higher cross-linking degree) (Table 1), the membranes fabricated from concentrations higher than 1.5/0.075 show hydrophilic properties with a CA around 60°. Further decreasing the m-XDA/TMC concentration leads to a decrease in the content of carboxyl groups (~1.6%) and an increase of the CA (Fig. 4b). Consequently, the m-XDA/TMC-1/0.05 and m-XDA/TMC-0.5/0.025 membranes exhibit a water CA of 103.1° and 98.3°, respectively, indicating their hydrophobic characteristics (Table 1). Livingston et al. prepared polyamide nanofilms by manipulating the monomer concentrations in a wide range of 0.0025–0.5 wt%.[12] It was found that even the

nanofilm prepared from an extremely low TMC concentration of 0.0025 wt% still maintained a hydrophilic surface with a CA smaller than 60°. By comparison, the introduced methylene endows the m-XDA/TMC membrane with tunable physico-chemical properties. The balance between the hydrophilic parts and the hydrophobic parts gives rise to a different hydrophilic/hydrophobic feature of the m-XDA/TMC membrane. All these composite membranes were found to have a negatively charged surface (Fig. 4c) with a zeta potential between −45 and −24 mV at neutral pH (Table 1). The carboxyl (–COOH) content in the PA thin film was confirmed from the O1s core level XPS spectra (Table S3†). The relationship between the zeta potential and the carboxyl group content is plotted in Fig. S9.† An overall trend could be found where a higher carboxyl content exhibits a lower zeta potential for the nanofilms except for the m-XDA/TMC-2/0.1 membrane, which has a lower zeta potential.

3.3 Organic solvent nanofiltration performance

There is a linear relationship between the permeance of the organic solvents and the reciprocal of the thickness of the selective PA layer (Fig. 5a). High permeances of 70.6 L m^{-2} L^{-1} bar^{-1} and 54.5 L m^{-2} L^{-1} bar^{-1} were achieved for DMF and acetone, respectively, when the PA thickness was 27 nm. In contrast, the permeances for the two aggressive solvents decreased to 9.1 L m^{-2} L^{-1} bar^{-1} (DMF) and 8.2 L m^{-2} L^{-1} bar^{-1} (acetone) when the PA thickness was 457 nm. These results demonstrate that controlling the monomer concentration allows us to effectively control the thickness of the molecular sieving nanofilm, determining the solvent permeability. Table 2 compares the organic solvent nanofiltration performance of m-XDA/TMC composite membranes. The m-XDA/TMC-3/0.15 membrane was found to have an almost complete rejection of rose Bengal (RB, 1017 g mol^{-1}, 100%) and methyl orange (MO, 327 g mol^{-1}, 99.6%) in acetone. The m-XDA/TMC-2/0.1 membrane had an acetone permeance two times higher than that of the m-XDA/TMC-3/0.15 membrane because of the decreased nanofilm thickness. In addition, the membrane still retained a high rejection for RB (99.9%) and a considerable rejection for MO (90.7%). The rejection for MO decreased and the permeability increased significantly when further deceasing the membrane thickness, indicating that the cross-linking degree of the selective layer was decreased. As shown in Table 1, a higher monomer concentration leads to a higher cross-linking degree but also results in a larger nanofilm thickness and vice versa. The interplay among the cross-linking degree, thin film thickness and separation performance (permeability and molecular selectivity) is regulated by manipulating the monomer concentration in the IP reaction. The solvent resistance of the m-XDA/TMC composite membrane was evaluated by immersing the membrane in various polar aprotic solvents, polar protic solvents and non-polar solvents for one week. It was found that dissolution of the crystalline particles on the membrane surface occurred in dimethyl sulfoxide and a strong swelling of the membrane in 1-methyl-2-pyrrolidinone and tetrahydrofuran was observed (Fig. S10†). However, the surface morphology of these composite membranes in mild alcoholic
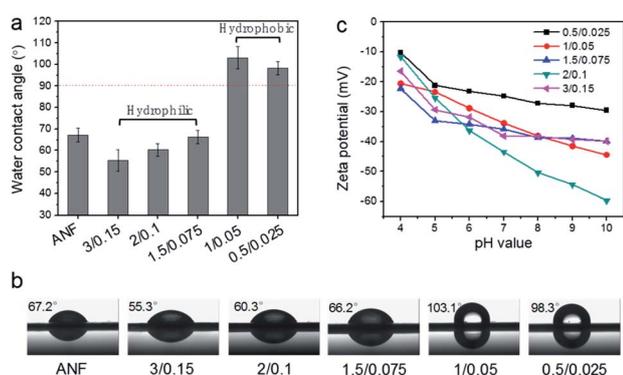

Fig. 4 (a) Contact angle of the ANF membrane and m-XDA/TMC composite membranes. (b) Photographs of the contact angle measurement. (c) Zeta potential of m-XDA/TMC composite membranes in the pH range of 4–10.

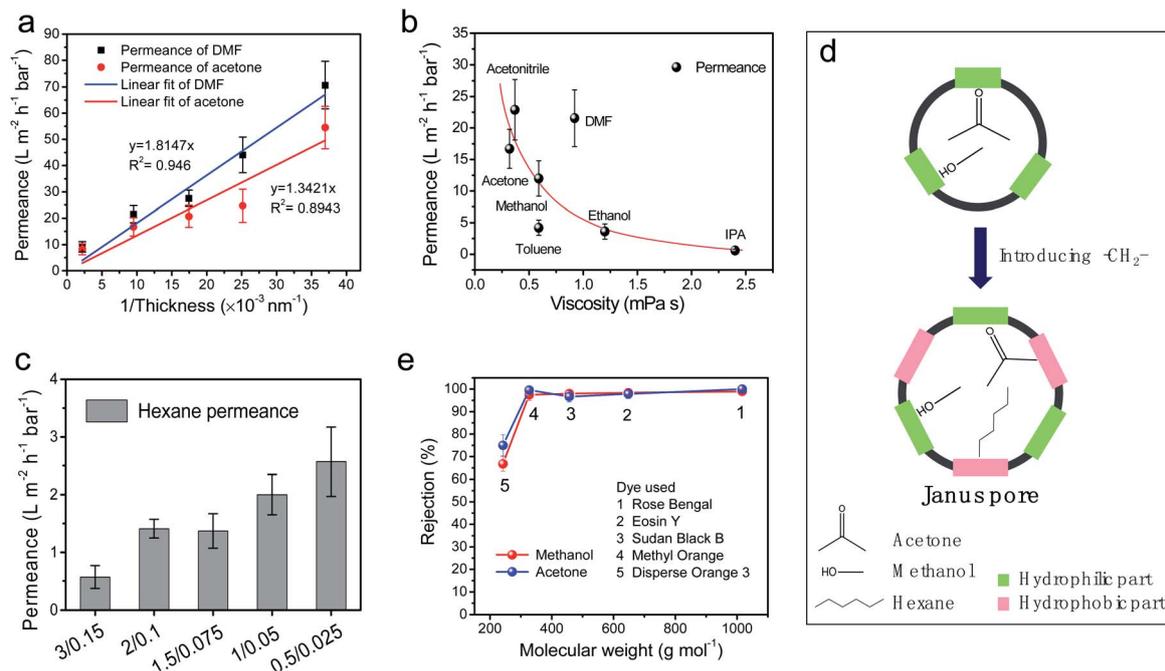Fig. 5 (a) The effect of membrane thickness on DMF and acetone permeance. (b) Pure solvent permeances *versus* the viscosity of the solvent for the *m*-XDA/TMC-2/0.1 composite membrane. (c) The *n*-hexane permeance of the *m*-XDA/TMC composite membranes. (d) The illustration of the Janus pore structure of the composite *m*-XDA/TMC membrane. (e) Rejection behavior of the *m*-XDA/TMC-3/0.15 composite membrane *versus* the molecular weight of various dyes (rose Bengal (RB, 1017 g mol^{-1}), eosin Y (EY, 648 g mol^{-1}), Sudan black B (SBB, 457 g mol^{-1}), methyl orange (MO, 327 g mol^{-1}) and disperse orange 3 (DO3, 242 g mol^{-1})) in acetone and methanol, respectively, with a molecular concentration of 20 mg L^{-1}.

solvents (methanol, ethanol, and isopropanol), acetone and non-polar solvents (toluene and *n*-hexane) was maintained after the treatment. The membrane permeance *versus* solvent viscosity is plotted in Fig. 5b. An inverse non-linear relationship between solvent permeance and solvent viscosity was observed, which is in accordance with the results reported elsewhere.[3,14] Due to the strong swelling effect of the hydrogel substrate, the membrane had a significantly higher permeance for DMF (21.6 L m^{-2} h^{-1} bar^{-1}) than for other solvents.[2] Because of the lower viscosity of acetonitrile (0.37 cP), acetone (0.32 cP) and methanol (0.59 cP), the permeances for these three polar solvents ranked the highest with 22.9, 16.7 and 12 L m^{-2} h^{-1} bar^{-1}, respectively. The membrane also showed a high

permeance for a non-polar solvent, *i.e.*, toluene (4.2 L m^{-2} h^{-1} bar^{-1}), which is over six times higher than that of commercial membranes (Starmem 122 and Starmem 144).[13,27] This permeance also surpasses that of most recently reported membranes, such as AlO$_x$/PIM-1,[28] cross-linked PVDF,[29] and epoxysilicone composite membranes.[30] To further demonstrate their potential application in non-polar solvents, the composite membranes were applied in *n*-hexane. It was found that the composite membrane had an increasing permeance for *n*-hexane from 0.6 to 2.6 L m^{-2} h^{-1} bar^{-1} (Fig. 5c). Notably, due to the hydrophilicity, a conventional polyamide membrane has a superior permeability for polar solvents, such as acetone and methanol, but extremely low permeances for non-polar

Table 2 Organic solvent nanofiltration performance of *m*-XDA/TMC composite membranes. Methyl orange (327 g mol^{-1}) and rose Bengal (1017 g mol^{-1}) dissolved in acetone with a concentration of 20 mg L^{-1} were used as the feed solution to study the solute rejection. Membranes were activated with DMF filtration for 10 min followed by filtration with a feed solution of acetone. The permeate was collected after the membrane was filtered for 30 min and the rejection was determined by UV-vis spectrophotometry. Nanofiltration experiments were performed in a dead-end stirred cell (600 rpm) at room temperature and 4 bar

Composite membrane	Pure acetone permeance (L m^{-2} h^{-1} bar^{-1})	Rose bengal (1017 g mol^{-1})		Methyl orange (327 g mol^{-1})	
		Permeance (L m^{-2} h^{-1} bar^{-1})	Rejection (%)	Permeance (L m^{-2} h^{-1} bar^{-1})	Rejection (%)
m-XDA/TMC-3/0.15	8.2	7.2	100	5.3	99.6
m-XDA/TMC-2/0.1	16.7	10.9	99.9	10.1	90.7
m-XDA/TMC-1.5/0.075	20.7	13.0	99.9	13.4	88.4
m-XDA/TMC-1/0.05	24.7	19.1	99.9	21.4	87.9
m-XDA/TMC-0.5/0.025	54.5	42.1	90.9	32.4	58.0

solvents, for example, *n*-hexane (<1 L m^{-2} h^{-1} bar^{-1}).[1,2,9,12,13] The comparison of the non-polar solvent (toluene and hexane) permeances of the *m*-XDA/TMC TFC membrane with those of other commercial OSN membranes and reported composite membranes in the literature are listed in Table S4.† The elevated non-polar solvent permeance for the *m*-XDA/TMC composite membrane can be attributed to the introduction of the alkyl (–CH$_2$–) group into the polyamide network, which has a good affinity towards *n*-hexane and toluene. In addition, the alternating distribution of the hydrophilic part and the hydrophobic part endows the membrane pores with Janus pathways, where the former represent the residual hydrolyzed carboxyl groups and amide groups, and the latter represents the introduced alkyl groups and the benzene rings (Fig. 5d). As a consequence, the Janus pathways facilitate the transport of both polar and non-polar solvents. To validate the interaction differences between the cross-linked polyamide polymer with different solvent molecules, the solubility parameter differences for the polymer and solvent are calculated, as shown in Tables S5 and S6.† Compared with conventional MPD/TMC polyamide, the *m*-XDA/TMC polyamide not only shows strong interactions with polar solvents (methanol, ethanol, and acetone) but also has better interactions with non-polar solvents (*n*-hexane and toluene). These results indicate that the *m*-XDA/TMC composite membranes are promising for use in nanofiltration of polar and non-polar solvents. The molecular weight cut-off (MWCO) of the *m*-XDA/TMC composite membranes was evaluated based on the rejection of different dye molecules in specific solvents (methanol and acetone). Dye molecules with different charges, molecular sizes and molecular weights are listed in Fig. S11.† A plot of rejection of dye molecules against molecular weight is presented in Fig. 5e. The composite membrane showed a similar MWCO between 242 and 327 g mol^{-1} in acetone and methanol, respectively. The UV-vis measurement results and the photographs of the feed/permeate in acetone are provided in Fig. S12.† Tables S7 and S8† also provide the permeance and rejection information of the MWCO experiment.

3.4 Stability test

The long-term filtration of the *m*-XDA/TMC composite membrane was evaluated in acetone, considered an aggressive solvent (Fig. 6a). The decrease of permeability is probably caused by physical ageing and compaction of the hydrogel composite membrane with DMF treatment.[2,19] Despite this, the *m*-XDA/TMC-3/0.15 membrane demonstrated an excellent nanofiltration separation ability in the long-term filtration experiment, in which a permeability of 5.2 L m^{-2} h^{-1} bar^{-1} was obtained for acetone with a rejection of 99.0% for methyl orange (MO, 324 g mol^{-1}). Fig. S13a† shows the UV-vis spectrum of the feed and permeate. The inset photo of the permeate indicates the highly efficient molecular separation capability of the *m*-XDA/TMC TFC membrane. As shown in Fig. S13b,† the membrane was compacted but no significant fouling is observed after the long-term filtration. These results demonstrate that the *m*-XDA/TMC TFC membrane has excellent stability in harsh organic solvents and has great potential for applications in solvent recovery, solute
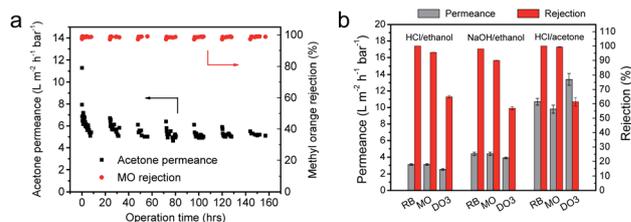

Fig. 6 (a) The long-term separation performance of the *m*-XDA/TMC-3/0.15 membrane in aggressive acetone using MO as the solute with a concentration of 100 mg L^{-1}. (Tested in a dead-end filtration cell in a batch experiment at 4 bar, 600 rpm at room temperature.) (b) The chemical stability of the *m*-XDA/TMC-2/0.1 composite membrane in harsh acidic and basic environments. The membranes were soaked in 0.1 M HCl water/ethanol, 0.1 M NaOH water/ethanol and 0.1 M HCl water/acetone, respectively, for 15 days. The membranes after treatment were tested using a dye/organic solution in ethanol and acetone, respectively.

concentration, *etc.* The OSN permeances of the *m*-XDA/TMC membrane are compared with those of other reported TFC membranes, as listed in Table S9.† The *m*-XDA/TMC TFC membrane developed in this work shows great advantages in terms of the high solvent permeances for both acetone and methanol as well as the excellent rejections for small organic molecules. The cross-linked aromatic framework and the introduced methylene groups endowed the *m*-XDA/TMC composite membranes with an extraordinary chemical stability, which is essential for OSN performance in harsh environments. The *m*-XDA/TMC-2/0.1 composite membranes were soaked in a variety of solutions under extreme conditions for 15 days: 0.1 M HCl in water/ethanol, 0.1 M NaOH in water/ethanol, and 0.1 M HCl in water/acetone. The OSN performances of the treated composite membranes were evaluated (Fig. 6b). The rejection of rose Bengal of these composite membranes remained almost 100% and high rejections of over 90% for MO both in ethanol and acetone were observed. Interestingly, the rejection for MO increased significantly from 90.7% to 99.4% after treatment with 0.1 M HCl in water/acetone. In contrast, the permeances for acetone remained stable. To investigate the stability of the membrane under more extreme conditions, the *m*-XDA/TMC-3/0.1 membranes were soaked under stronger acidic and basic conditions for 15 days: 0.5 M HCl in water/ethanol, 0.5 M NaOH in water/ethanol, and 0.5 M and 1 M HCl in water/acetone. As shown in Fig. S14a,† the color of the membrane immediately changed to pink in HCl/acetone and yellow in NaOH/ethanol but remained the same in HCl/ethanol. Despite the color change, the membrane exhibited excellent molecular rejections for RB (100%) and MO (>98%) in ethanol and acetone, respectively (Fig. S14b†). The surface morphology of these composite membranes after filtration with MO/solvent was examined and maintained well according to SEM observations (Fig. S14c†). In addition, the chemical stability of the thinnest membrane (*m*-XDA/TMC-0.5/0.025) was also investigated under harsh conditions (Fig. S15†). The results show that the *m*-XDA/TMC composite membrane even with a thickness down to 27 nm can still maintain its separation efficiency under harsh conditions. The chemical stability of the *m*-XDA/TMC composite membranes can be attributed to the robust nature of

the aramid nanofibers and the introduced inert alkane chain of the PA layer. This allows for the membrane to be used in practical applications in organic liquids and in harsh environments containing strong acids/bases.

4. Conclusions

In summary, a novel polyamide membrane with Janus pore structures was prepared. The alkyl ($-CH_2-$) group was facilely introduced into the hydrophilic cross-linked polyamide network *via in situ* interfacial polymerization. The membrane showed a controllable surface morphology, nanofilm thickness, cross-linking degree and surface hydrophilicity by varying the monomer concentrations. The nanofilm thickness has an inverse relationship with the solvent permeability in a range between 27 nm and 457 nm. The membrane surface hydrophilicity shifted from hydrophilic (CA: 55.3°) to hydrophobic (CA: 103.1°) with decreasing monomer concentrations. The introduced alkyl group and the polyamide constitute the Janus pore structure, providing a good affinity to both polar and non-polar solvents. As a result, the Janus pathway leads to high permeances for polar solvents (acetonitrile: 22.9 L m^{-2} h^{-1} bar^{-1}, acetone: 16.7 L m^{-2} h^{-1} bar^{-1}, and methanol: 12.0 L m^{-2} h^{-1} bar^{-1}) and superior permeances for non-polar solvents (*n*-hexane: 0.6–2.6 L m^{-2} h^{-1} bar^{-1} and toluene: 4.2 L m^{-2} h^{-1} bar^{-1}). The composite membrane showed excellent molecular sieving properties, with a MWCO of 242–327 g mol^{-1}. Benefiting from the inert alkyl groups, the membrane has a good chemical stability in both strongly acidic and strongly basic environments for at least 15 days. Given the outstanding chemical stability, excellent permeability and selectivity, the *m*-XDA/TMC composite membrane emerges as a promising candidate for versatile OSN applications in polar and non-polar solvents as well as under extreme conditions.

Conflicts of interest

There are no conflicts to declare.

Acknowledgements

Notes and references

1 P. Marchetti, M. F. Jimenez Solomon, G. Szekely and A. G. Livingston, *Chem. Rev.*, 2014, **114**, 10735–10806.

2 Y. Li, E. Wong, A. Volodine, C. Van Haesendonck, K. Zhang and B. Van der Bruggen, *J. Mater. Chem. A*, 2019, **7**, 19269–19279.

3 Y. Li, S. Yuan, C. Zhou, Y. Zhao and B. Van der Bruggen, *J. Mater. Chem. A*, 2018, **6**, 22987–22997.

4 B. Liang, X. He, J. Hou, L. Li and Z. Tang, *Adv. Mater.*, 2018, e1806090, DOI: 10.1002/adma.201806090.

5 C. Wang, C. Li, E. R. C. Rutledge, S. Che, J. Lee, A. J. Kalin, C. Zhang, H.-C. Zhou, Z.-H. Guo and L. Fang, *J. Mater. Chem. A*, 2019, DOI: 10.1039/c9ta10190j.

6 B. A. Pulido, C. Waldron, M. G. Zolotukhin and S. P. Nunes, *J. Membr. Sci.*, 2017, **539**, 187–196.

7 P. Gorgojo, S. Karan, H. C. Wong, M. F. Jimenez-Solomon, J. T. Cabral and A. G. Livingston, *Adv. Funct. Mater.*, 2014, **24**, 4729–4737.

8 L. Xia, J. Ren, M. Weyd and J. R. McCutcheon, *J. Membr. Sci.*, 2018, **563**, 857–863.

9 M. F. Jimenez Solomon, Y. Bhole and A. G. Livingston, *J. Membr. Sci.*, 2013, **434**, 193–203.

10 J. Liu, D. Hua, Y. Zhang, S. Japip and T. S. Chung, *Adv. Mater.*, 2018, **30**, 1705933.

11 M. F. Jimenez-Solomon, Q. Song, K. E. Jelfs, M. Munoz-Ibanez and A. G. Livingston, *Nat. Mater.*, 2016, **15**, 760–767.

12 S. Karan, Z. Jiang and A. G. Livingston, *Science*, 2015, **348**, 1347–1351.

13 M. F. Jimenez Solomon, Y. Bhole and A. G. Livingston, *J. Membr. Sci.*, 2012, **423–424**, 371–382.

14 B. Liang, H. Wang, X. Shi, B. Shen, X. He, Z. A. Ghazi, N. A. Khan, H. Sin, A. M. Khattak, L. Li and Z. Tang, *Nat. Chem.*, 2018, **10**, 961–967.

15 K. Dey, M. Pal, K. C. Rout, H. S. Kunjattu, A. Das, R. Mukherjee, U. K. Kharul and R. Banerjee, *J. Am. Chem. Soc.*, 2017, **139**, 13083–13091.

16 T. Huang, T. Puspasari, S. P. Nunes and K. V. Peinemann, *Adv. Funct. Mater.*, 2020, **30**, 1906797.

17 Y. Liu, B. Lin, W. Liu, J. Li, C. Gao and Q. Pan, *RSC Adv.*, 2018, **8**, 36430–36440.

18 R. Othman, A. W. Mohammad, M. Ismail and J. Salimon, *J. Membr. Sci.*, 2010, **348**, 287–297.

19 Y. Li, E. Wong, Z. Mai and B. Van der Bruggen, *J. Membr. Sci.*, 2019, 592.

20 Y. Li, S. Li and K. Zhang, *J. Membr. Sci.*, 2017, **537**, 42–53.

21 Y. Li, S. Yang, K. Zhang and B. Van der Bruggen, *Desalination*, 2019, **454**, 48–58.

22 C. Su, L. Chi, Y. Qian, S. Sun and Z. Jiang, *J. Mater. Sci. Chem. Eng.*, 2018, **06**, 1–15.

23 S. K. Karode, S. S. Kulkarni, A. K. Suresh and R. A. Mashelkar, *Chem. Eng. Sci.*, 1998, **53**, 2649–2663.

24 Z. Jiang, S. Karan and A. G. Livingston, *Adv. Mater.*, 2018, **30**, e1705973.

25 V. T. Do, C. Y. Tang, M. Reinhard and J. O. Leckie, *Environ. Sci. Technol.*, 2012, **46**, 852–859.

26 Y. Li, C. Li, S. Li, B. Su, L. Han and B. Mandal, *J. Mater. Chem. A*, 2019, **7**, 13315–13330.

27 D. Fritsch, P. Merten, K. Heinrich, M. Lazar and M. Priske, *J. Membr. Sci.*, 2012, **401–402**, 222–231.

28 E. K. McGuinness, F. Zhang, Y. Ma, R. P. Lively and M. D. Losego, *Chem. Mater.*, 2019, **31**, 5509–5518.

29 M. Mertens, C. Van Goethem, M. Thijs, G. Koeckelberghs and I. F. J. Vankelecom, *J. Membr. Sci.*, 2018, **566**, 223–230.

30 M. Cook, L. Peeva and A. Livingston, *Ind. Eng. Chem. Res.*, 2018, **57**, 730–739.